Heliyon 10 (2024) e29192

Contents lists available at ScienceDirect

Heliyon

journal homepage: www.cell.com/heliyon

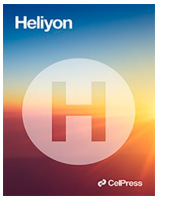

Research article

Enhancing piezoelectric effect of PVDF electrospun fiber through NiO nanoparticles for wearable applications

Bindhu Amrutha , Arun Anand Prabu [*], Madhvesh Pathak [**]

Department of Chemistry, School of Advanced Sciences, Vellore Institute of Technology, Vellore, 632014, India

ARTICLE INFO

Keywords:
Polyvinylidene fluoride
Nickel oxide
Electrospinning
Piezoelectric nanogenerator
Wearable applications

ABSTRACT

Flexible electrospun fiber-based piezoelectric nanogenerator (PENG) has attracted a lot of interest due to its ability of generating electrical energy from mechanical energy sources. The present work aims to improve the piezoelectric output of PENG devices based on electrospun polyvinylidene fluoride (PVDF) doped with nickel oxide nanoparticles (NiO NPs) in different concentrations (2, 4, 6, 8 and 10 wt.-%). Crystalline phase changes and β-crystalline content in electrospun fibers were evaluated using XRD and FTIR-ATR, respectively. Surface morphology and surface roughness of the electrospun fibers were observed using FE-SEM and AFM, respectively. The hydrophobic nature of the fibers was analyzed using a wettability test. PENG output voltage and short-circuit current performance of neat PVDF and PVDF doped with NiO (PN) composite electrospun fibers were calculated using a customized variable-pressure setup with an optimized force of 1.0 kgf and 1.0 Hz frequency. Neat PVDF-based PENG exhibited only 1.7 V and 0.7 μA, whereas, PVDF doped with 6 wt.-% NiO NP (PN-6) based PENG generated a high output voltage of 5.5 V and 1.83 μA current. The optimized PN-6 PENG device is demonstrated for use in wearable devices towards identifying certain body movements like tapping, wrist movement, walking and running.

1. Introduction

In recent times, smart electronic devices with excellent receptivity have attracted the attention of industries focusing on smart devices, flexible and portable sensors, electronic skins and wearable technology [1–4]. The challenge of finding a way to continuously power these gadgets is still unanswered, despite the fast development of advanced electronic devices [5]. Conventional batteries fall short of meeting the demands of contemporary electronic gadgets because of their low power density and limited life span. As a result, studies on electronic gadgets with self-sustaining systems have sparked a lot of attention in recent years. A common example of self-sustaining electronics is the piezoelectric nanogenerator (PENG) with excellent output voltage efficiency [6–9]. In general, piezoelectric materials are classified under two distinct categories: inorganic and organic materials. The first type consists of lead zirconate titanate [10], zinc oxide (ZnO) [11], barium titanate ($BaTiO_3$) [12] and potassium niobate [13]. The second type consists of cellulose [14,15], nylon-11, polyacrylonitriles [16], fluoropolymers such as polyvinylidene fluoride (PVDF) [17], copolymers like PVDF-*co*-hexafluoropropylene (PVDF-HFP) [18,19] and PVDF-co-trifluoroethylene (P(VDF-TrFE)) [20]. Ceramic-based piezo materials are hard and extremely brittle, despite having high coefficients of piezoelectric and dielectric properties, making them unsuitable

* Corresponding author.
** Corresponding author.
E-mail addresses: anandprabu@vit.ac.in (A. Anand Prabu), madhveshpathak@vit.ac.in (M. Pathak).

https://doi.org/10.1016/j.heliyon.2024.e29192
Received 29 January 2024; Received in revised form 1 April 2024; Accepted 2 April 2024
Available online 5 April 2024

in piezoelectric energy harvesting applications. Some polymers with piezo properties can overcome this obstacle by being more flexible and exhibiting better tensile strength [21].

A variety of PVDF-based sensors as energy harvesting systems have been reported due to their many advantages such as flexible structure, ecological sustainability, strongly biocompatible, chemically inert, lower acoustic resistance and superior piezoelectric characteristics [22,23]. PVDF is a thermoplastic polymer consisting of five different crystalline phases (α, β, γ, δ and ε) [24], where α-phase is the only non-polar crystalline phase [25]. Compared to other phases, the β-crystalline structure exhibits a significantly higher dipole moment aided by the all-trans arrangement of F and H atoms along the carbon backbone [26,27]. Furthermore, a variation in the value of electronegativity that exists between the atoms of H and F results in exceptional piezoelectric and ferroelectric properties [28]. The polar β-crystalline phase can be obtained through a variety of methods like high-pressure crystallization [29], uniaxial stretching [30], electric poling [31], annealing [32], electrospinning [33] and addition of nanofillers [27,34,35].

Over the last few decades, a wide range of methodologies for producing PVDF fibers have been established, and among them, melt-spinning and electrospinning are the two most prevalent methods. Melt-spinning produces less porous fibers with highly regulated fiber diameter but with randomly aligned molecular dipoles, which requires post-treatment. Electrospinning is a simple, rapid, adaptable and effective process for producing nanofibers (NFs). To produce the fiber with appropriate size and morphology, exact monitoring of operating parameters is required throughout the electrospinning procedure. The electrospun NFs exhibit unique properties such as nanoscale fiber diameter, large surface area and highly porous fiber. During the electrospinning process, simultaneous unidirectional stretching and electrical poling on the polymer chain result in the favorable formation of the polar crystalline phase, which is a key factor for enhancing the piezoelectric characteristics of the PENG device [36,37].

Recent studies have demonstrated that doping of several inorganic fillers like piezoelectric ceramics, metal and metal oxide nanoparticles (NPs) leads to the enhancement of β-phase in PVDF. Dhakras et al. [38] reported improved piezoelectric properties in electrospun PVDF fiber with the addition of $NiCl_2{\cdot}6H_2O$ hydrated salt. They found a 30 % increase in polar β-phase in the composite fiber and a peak-to-peak output voltage ($V_{p\text{-}p}$) of 0.76 V. Chen et al. [39] developed graphene oxide doped PVDF electrospun nanocomposite fiber-based PENG having a high output voltage of 1.1 V. Using the electrospinning process, Bairagi and Ali [40] developed a novel piezoelectric nanocomposite comprising ZnO and potassium sodium niobate (KNN) loaded PVDF. Based on their findings, both KNN and ZnO-doped PVDF PENG have the highest voltage output than other combinations such as PVDF-ZnO and PVDF-KNN. Yempally et al. [4] developed a self-powered PENG device using Zn–Fe_2O_3 doped PVDF electrospun fiber with a reported voltage of 0.41 V for 3 wt.-% nanofiller doped fiber. Dutta et al. [41] developed a lightweight and flexible NiO/PVDF solution casted film for EMI shielding applications. In another study, they reported NiO@SiO_2-doped PVDF nanocomposite film for EMI shielding and UV protection applications [42]. However, these film-based TENGs are not flexible and are highly brittle. Among the NPs used in earlier studies, PVDF doped with NiO NP exhibits exceptional capacity to adjust magnetic, mechanical and electrical behavior without impacting fiber flexibility. Superior storage capacitance and transport characteristics of NiO are the main driving force for its wider application in wearable sensors. Venkatesan et al. [43] reported NiO/PVDF electrospun fiber-based TENG for energy harvesting applications. As per our knowledge, there aren't any studies on electrospun NiO-doped PVDF PENG for wearable applications, and we didn't use any difficult synthesis methods or other surface treatments. The synthesis of NiO NP and NiO-doped PVDF electrospun fiber

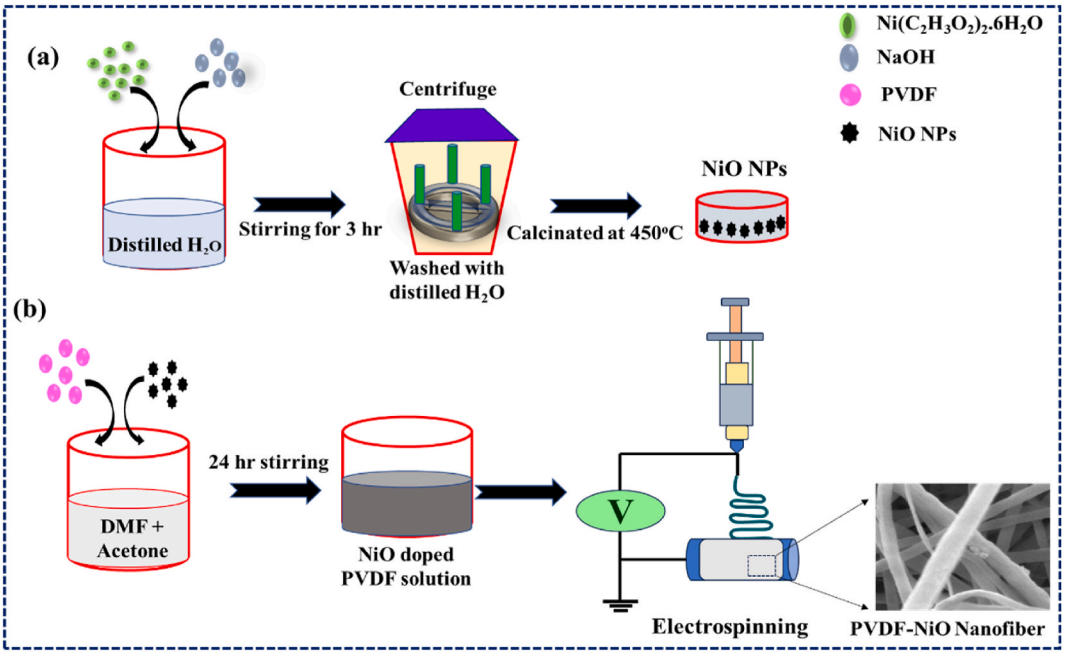

Fig. 1. (a) Graphic illustration of the synthesis of NiO NP and (b) fabrication of NiO-doped PVDF-based electrospun fiber.

is the main objective of the study. Ultimately, the fibers were utilized in the fabrication of PENG and in wearable applications.

Motivated by these findings, we focused on preparing varying weight % of NiO NP-doped PVDF electrospun fiber for use as a PENG sensor. Doping of NiO NP in PVDF results in enhanced polar electroactive β-phase compared to neat PVDF along with improved piezoelectric properties in both longitudinal and transverse directions. The PENG device is fabricated by stacking the nanocomposite fiber layer between two electrodes. By applying a force of 1.0 kgf, the sensor gave $V_{p\text{-}p}$ of 5.5 V which is 3.5 times higher than that of the neat PVDF-based PENG. Additionally, the PENG is used to identify and distinguish between various human body movements like walking, running, kicking, finger tapping and wrist bending. This finding shows that the developed PENG has a wide range of practical applications for self-sustaining wearable smart textiles.

2. Experimental section

2.1. Reagents

PVDF powder (M_w = 370,000 g mol^{-1}) was bought from Solvay, Korea. 98 % sodium hydroxide (NaOH) and nickel acetate hexahydrate ($Ni(C_2H_3O_2)_2{\cdot}6H_2O$) were purchased from Sigma Aldrich. Dimethylformamide (DMF) and acetone were purchased from Merck. The polyester-based Ni–Cu electrode was bought through Solueta Co. Ltd. Korea. All materials were stored in a clean, dry well-ventilated area and the containers were kept well closed. All the reagents were employed in the studies without further purification.

2.2. Synthesis of NiO NP

A simple chemical co-precipitation approach was used in the synthesis of NiO NPs. $Ni(C_2H_3O_2)_2{\bullet}6H_2O$ was mixed with double distilled water to prepare 0.1 M solution and kept under continuous stirring at room temperature for 2 h. Further, 0.1 M NaOH solution was added into the Ni solution till the pH reached around 14 and left undisturbed for 24 h. The formed precipitate is recovered by centrifugation and rinsed multiple times with distilled water to reduce the pH to 7. The resultant product was subsequently dried for 12 h at 80 °C in a hot air oven and further calcined for 5 h at 550 °C in a muffle furnace (Fig. 1(a)). The final product was examined through Field emission-scanning electron microscopy (FE-SEM), X-ray diffraction (XRD) and Fourier transform-infrared spectroscopy (FTIR) techniques [44,45].

2.3. Fabrication of NiO-doped PVDF nanocomposite fiber

Initially, five different wt.-% of NiO NP (2, 4, 6, 8 and 10 wt.-%) were dispersed in DMF/acetone (6:4) solvent mixture for 30 min under magnetic stirring. PVDF powder was added to the NiO suspension, and the resulting solution was thoroughly dispersed with magnetic stirring over 3 h at 40 °C. The concentration of PVDF was set at 12 wt.-% in all the prepared solutions. The fibers were fabricated using the simple and facile electrospinning technique. The homogeneous polymer nanocomposite solution was filled in a syringe fitted with a 23 G needle and injected at a flow rate of 1.2 ml/h during electrospinning. A DC power source was used to apply a high voltage of 20 kV to the needle tip, which results in the transformation of the solution into a Taylor cone. The formed NFs were collected upon a Teflon sheet that was covered around the cylindrical drum that rotates at a speed of 70 rpm and placed 10 cm away from the tip of the needle. After 6 h of spinning, the NF is collected and used for further measurements. Fig. 1(b) depicts the steps involved in the preparation of the NFs.

2.4. Characterization

The crystalline phase structure and particle size of NiO NP were analyzed from XRD patterns measured at room temperature using Cu-Kα radiation with a wavelength of 1.54 Å and 2θ range of 20°–90°. The presence of functional groups in NiO NP was verified using FTIR technique. Surface morphology of the synthesized NP was analyzed using FE-SEM and EDS mapping. Crystalline structure of the electrospun neat PVDF and its composite fibers were characterized using XRD and FTIR. FTIR spectrum was acquired within 400–4000 cm^{-1} wavenumber regions. FE-SEM and EDS mapping were used to examine the morphological and elemental composition of the electrospun fibers. Topography of the electrospun NFs was analyzed using atomic force microscopy (AFM). Water contact angle (WCA) of the electrospun fibers were analyzed using the sessile drop method coupled with KRÜSS ADVANCE software. Sessile drop method is used to study the behavior of liquid drops over solid materials, and is correlated with KRÜSS ADVANCE software for easier drop shape assessment and contact angle analysis. To generate a piezoelectric signal, a custom-made dynamic compression study configuration was used on the fabricated sensors with a minimum force of 0.1 kgf to the highest force of 3.0 kgf. The piezoelectric signals produced by the sensors during repeated loading and unloading process sessions were recorded in $V_{p\text{-}p}$ form using an input impedance of 100 MΩ, 20 dB gain and frequency range of 0.1–1.0 Hz. The optimized voltage was measured at 1.0 kgf force and 1.0 Hz frequency. Data collecting, recording and analyzing were accomplished using an NI-DAQ device linked to a computer *via* LabVIEW software. Piezoelectric signals captured during human body movements were obtained as a coefficient of time by employing a BIOPAC MP-150 recording system under identical conditioning parameters such as 100 MΩ and 20 dB gain, and recorded in the system using Acknowledge 4.2 software.

2.5. Fabrication and mechanism of PENG device

Initially, the fabricated NF was sliced into little pieces having a 2 × 2 cm^2 effective working surface. Then, the fiber membrane was sandwiched between two flexible Ni–Cu electrodes. Finally, the complete device was wrapped using a PET sheet to protect it from external disturbances and improve output efficiency. Fig. 2(a and b) depicts the material arrangement in PENGs. After polarization, a reversible charge develops along the corresponding top and bottom sides of the piezoelectric material layers.

Fig. 2(c) depicts the working mechanism of PENG. Piezoelectric effect is the basis for the working of piezoelectric transducers when tension or deformation is applied to a crystalline polarized material. The molecular geometry of a material is subsequently altered by the stress, which either creates or modifies the polarity of the material and is comparable with dielectric effect. This happens when the movement of electrons within an insulator generates a charge. P_S represents polarity and the vector's length denotes its strength. Current flows in the same direction as the polarity of the crystal when the polarity is decreased, and the current flows in the opposite direction when the polarity is increased [46,47].

3. Results and discussion

3.1. Characterization of NiO NP

Fig. 3 (a,b) shows the SEM image of NiO NP under two different magnification scales (300 nm and 500 nm) with a spherical and uniformly distributed morphology. Fig. 3(c and d) shows EDS mapping of the prepared NiO NP with an average size of 20 nm as observed through the histogram in Fig. 3(e). Fig. 3(f) depicts the XRD pattern of NiO NP. The intensity peaks found at 37.2°, 43.2°, 62.8°, 75.4° and 79.3° agreed with the Miller indices patterns of crystallographic peaks (101), (012), (110), (113) and (202) which suited with the JCPDS card number 00-004-0835. Mean particle size of the NP was computed using Scherer equation as shown in Eq. (1).

$$D_{h,k,l} = 0.9\lambda / (\beta_{h,k,l} \cos\Theta) \quad (1)$$

Where, 0.9 is shape factor value; λ is the employed X-ray beam wavelength (~1.54 Å); Θ is the diffraction angle; and β is the diffraction peak's full width at half maximum [42]. The average particle size of NiO NP corresponding to the highest peak exhibited in XRD was calculated to be around 18 nm, which correlates with the particle size analyzed from the histogram study. The formed NP was in a very pure state, and the XRD pattern shows significant structural peaks as well as particles having diameters less than 100 nm range.

Fig. 3(g) shows the FTIR spectra of NiO NP, which confirms the O–H stretching absorption band at 3400 cm^{-1} and C–H stretching band at 2885 cm^{-1}. Hydroxyl group absorption was observed at 1600 cm^{-1} and the presence of carbonates were detected by bands at 1378 cm^{-1} and 1104 cm^{-1}. The absorption at 830 cm^{-1} is assigned to the bending of C–H bond and the Ni–OH stretching band appears at 615 cm^{-1}. The characteristic peaks were very similar to the values reported in earlier literature [41]. From XRD and FTIR results we confirmed the successful synthesis of NiO NP with a desirable particle size.

3.2. Characterization of NiO NP doped PVDF electrospun fiber

3.2.1. XRD analysis

XRD analysis verified the increase of the β-crystalline phase in NP-doped PVDF fiber relative to the undoped PVDF fiber. The

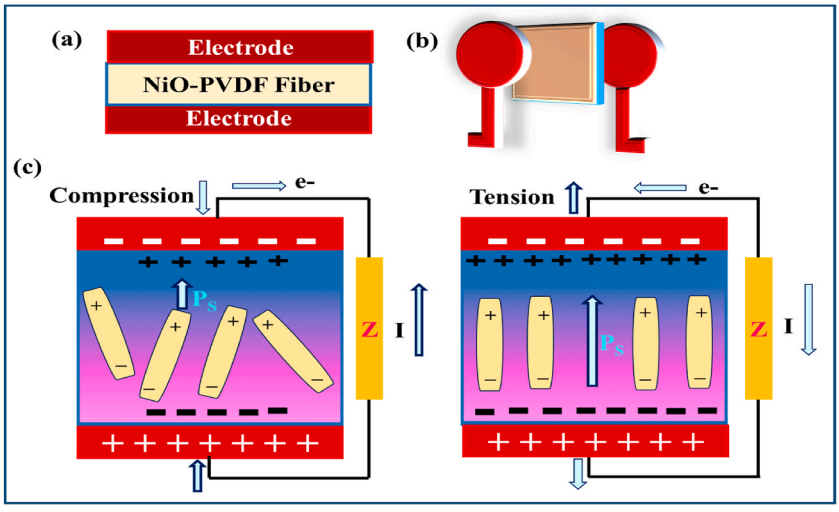

Fig. 2. (a,b) Graphic depiction of the layer alignment and (c) Charge generation process in the PENG device.

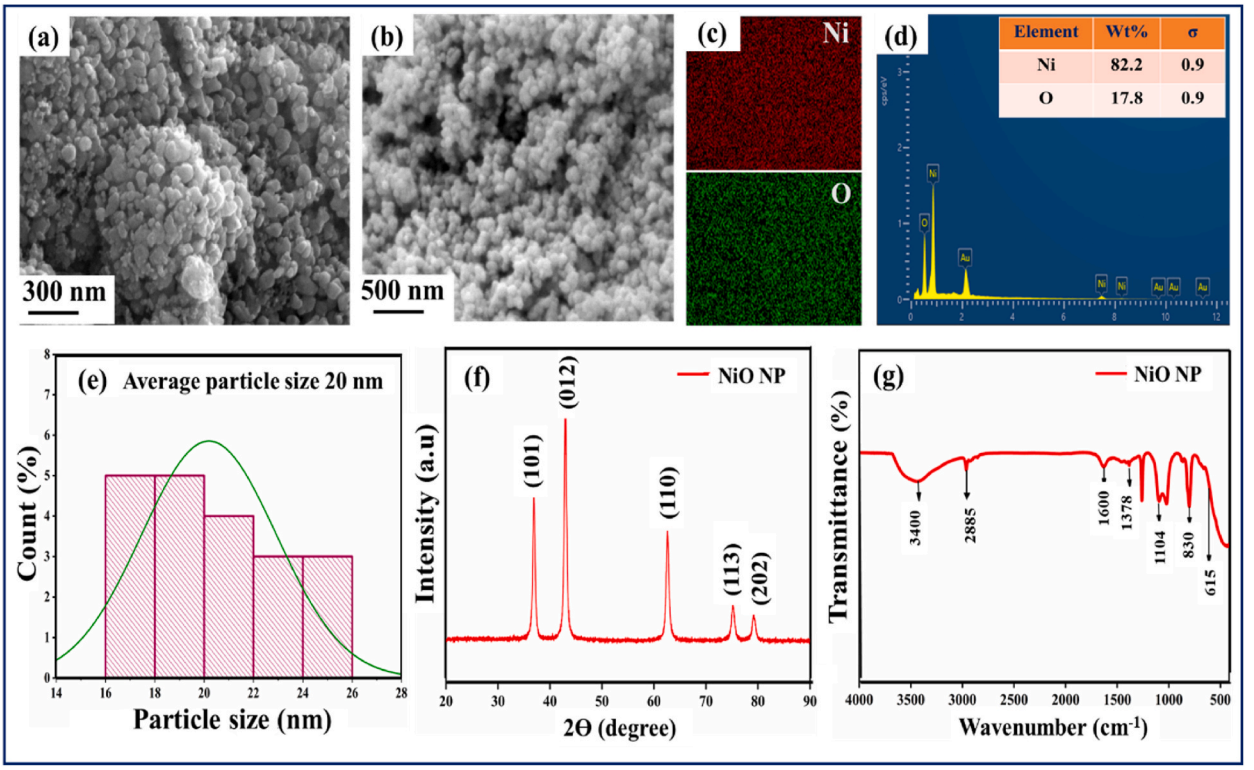

Fig. 3. (a–b) FE-SEM images under two different magnification scales (300 nm and 500 nm), (c–d) Elemental mapping, (e) Histogram profile, (f) XRD structural characterization and (g) FTIR pattern of NiO NP.

diffraction peaks of PVDF electrospun fiber with and without NP doping are shown in Fig. 4(a). The fibers exhibited a strong diffraction peak at 20.4° corresponding to the polar β-phase. A faint peak at 18.4° related to the existence of the non-polar α-phase, although its strength is reduced corresponding to the increased doping of NP into PVDF. This can be attributed to the nucleation effect facilitated by the incorporation of NP in PVDF, which encourages the transition from α-to β-phase in PVDF. The charged NiO NP shifts the dipole patterns of PVDF from *trans-gauche-trans-gauche* conformation to *all-trans* conformation during the process of β-phase nucleation. NiO NP doped fibers showed two additional minor peaks at 37° and 48°, proving the presence of NP in PVDF fiber. But the addition of 10 wt.-% NiO NP in PVDF showed a combined peak rather than two distinct peaks, which could be attributed to NP clustering within the PVDF fiber. The crystalline nature of the fibers and the enhanced β-phase were confirmed after the doping of NiO NP.

3.2.2. FTIR-ATR analysis

FTIR spectroscopy was used to study the crystalline nature of the fabricated NP-doped PVDF electrospun fiber. FTIR studies confirmed the formation of polar β-phase in the PVDF composite electrospun fibers as shown in Fig. 4(b). The spectra of neat PVDF fiber exhibit predominantly non-polar α-crystalline phase band at 490 cm^{-1} assigned to the CF_2 bond waging, 530 cm^{-1} band assigned to the bending of the CF_2 bond, peaks at 615 and 765 cm^{-1} responsible for the skeletal bending of CF_2, and CH_2 rocking responsible for the absorption bands at 796 and 975 cm^{-1}. The addition of NiO NP into the PVDF matrix results in the total reduction of non-polar α-crystalline peaks. Development of bands observed in the NiO/PVDF fibers at 510, 600, 840 and 1278 cm^{-1} corresponds to the deformation of CF_2 bonds, CF_2 stretching, CF_2 wagging and CH_2 rocking, respectively. These bands confirm the formation of the β-crystalline phase [48,49]. 1072 cm^{-1} represents the thickness-related peak. Using Beer-Lambert law, the percentage of β-phase (F(β)) in the fabricated fibers were computed as given in Eq. (2).

$$F(\beta) = [(A_\beta)/((1.26 \times A_\alpha) + A_\beta)] \times 100 \quad (2)$$

Where, A_α and A_β represent the absorption bands for 765 cm^{-1} and 840 cm^{-1}, respectively. The estimated F(β%) is shown graphically in Fig. 4(c) and Table S1 in Supporting information (SI). A maximum of 70 % increase in the β-phase was obtained with the addition of 6 wt.-% NiO NP in PVDF matrix (PN-6). From the FTIR study, the percentage increase of the β-crystalline phase was confirmed.

3.2.3. FE-SEM of NiO-PVDF fiber

Fig. 4(d–f, h, j, l and n) illustrates the FE-SEM images of NiO NP doped PVDF electrospun NF materials of compositions PN-0, PN-2, PN-4, PN-6, PN-8 and PN-10, respectively. Histogram analysis of the neat and composite fibers is shown in Fig. 4(e–g, I, k, m and o).

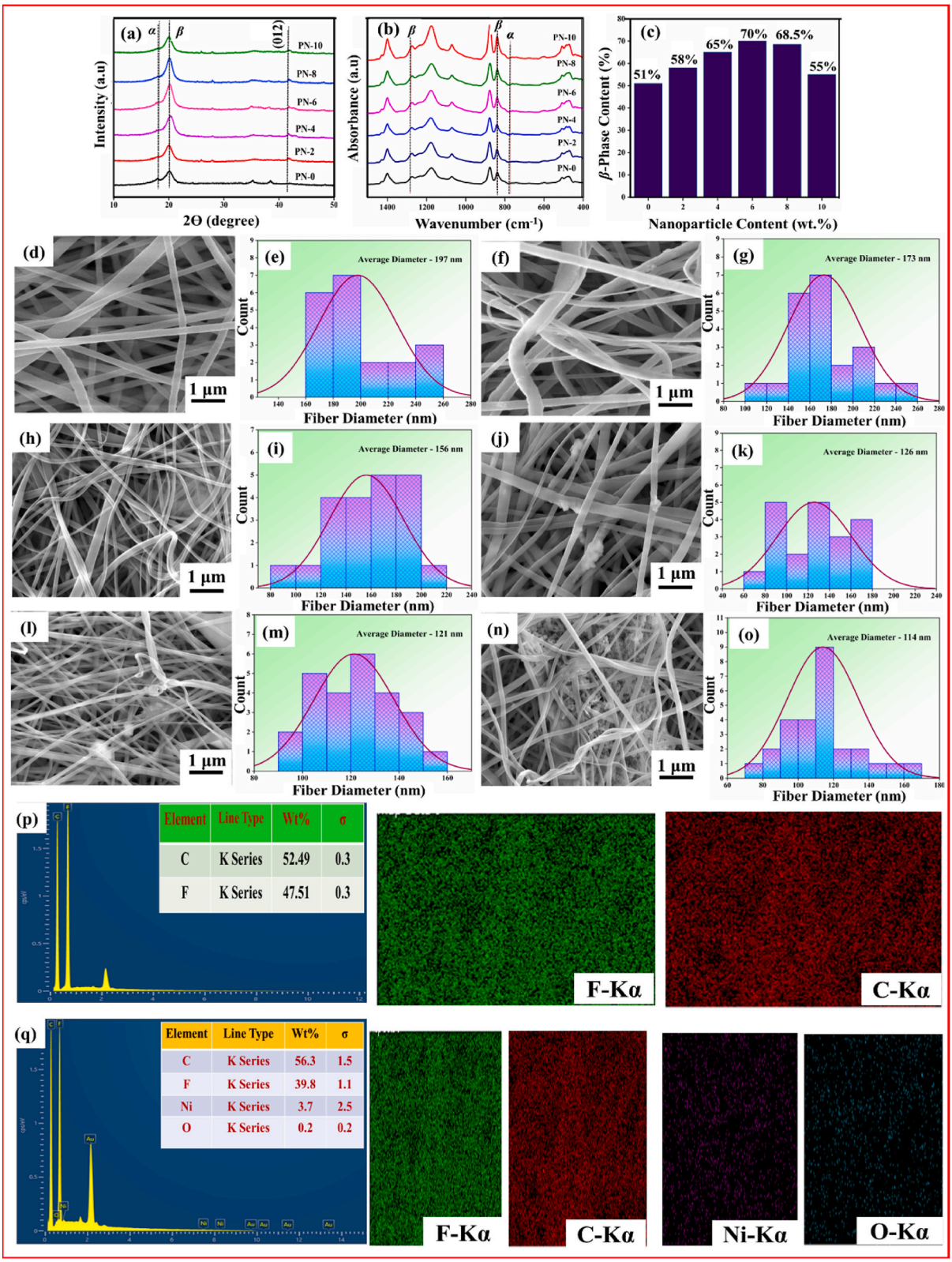

Fig. 4. (a) XRD pattern and (b) FTIR spectra of neat PVDF and various ratios of NiO NP doped PVDF electrospun fibers. (c) *β*-phase fraction values of NiO NP doped PVDF electrospun fibers extracted from (b). (d, f, h, j, l and n) FE-SEM images of PN-0, PN-2, PN-4, PN-6, PN-8 and PN-10. (e, g, I, k, m and o) histogram analysis of the corresponding fibers. (p, q) EDS mapping of PN-0 and PN-6 electrospun fiber, respectively.

The PN-0 fiber shows an average fiber diameter of 197 nm, and thereafter, the average fiber diameter varies from 173 nm to 114 nm. With increasing weight % of NiO NP in the PVDF matrix, the electrospun NF's average diameter decreased, which could be due to the rise in polymer solution's conductivity with increasing concentrations of NiO NP [50]. The NF thickness could also be reduced due to the change in viscoelastic characteristics of the spinning solution with increasing NiO wt.-% in PVDF. Fig. 4(j) exhibits an even fiber arrangement, and the uniform dispersion of NiO NP in the surface of PVDF was confirmed using EDS mapping from Fig. 4(q). Increasing the doping of NiO NP wt.-% in PVDF matrix from 8 to 10 resulted in the formation of agglomerated NF as shown in Fig. 4(l and n). Agglomeration frequently happens in composite electrospinning when the polymer solution has a large concentration of particles. The dispersion stages performed in the preparatory procedures before fiber production determine these agglomerations. The surface morphology of the fibers and their diameter were measured from the FE-SEM analysis. After the doping of the NiO NP the diameter became less, and the NP doping in the PVDF surface were also confirmed.

3.2.4. AFM study of NiO-PVDF fiber

With the help of 2-D and 3-D images of AFM, we were able to assess and compare the surface roughness of neat PVDF and PN composite NFs (Fig. 5). The surface roughness (R_a), root mean square roughness (R_q), valley depth (R_v) and peak height (R_p) of neat PVDF and PN composite NFs are listed in Table S2 of SI. PN-0, PN-2, PN-4 and PN-6 showed R_a values of 170 nm, 282 nm, 357 nm and 1908 nm, respectively. Increasing NP addition in PVDF leads to an increase in R_a value. These findings demonstrate that the PN-6 fiber has a higher R_a value than all other fabricated fibers. This could have resulted in an effective increase of surface area with increasing surface roughness, which may let more charges to accumulate over the surface and also produce additional charges on the surface. After the doping of NP, an increased surface roughness was confirmed from the AFM analysis, which is a crucial factor for electrical study.

3.2.5. WCA measurement

Materials having hydrophilic surfaces tend to absorb surrounding moisture air, resulting in the formation of a thin water molecules layer that spreads across the fiber surface, which could affect its electrical properties. Therefore, the hydrophobicity/hydrophilicity of the undoped PVDF and doped NP nanofibers were examined by WCA measurements. After being cut into 1 cm × 1 cm size, each fiber was fixed to a slide, and 3 μL droplet of deionized water was poured over the fiber's surface. WCA values were evaluated every 10 s and Fig. 6(a–f) shows the WCA of neat and composite fibers. WCA measurements for PN-0, PN-2, PN-4, PN-6, PN-8 and PN-10 composite NFs were 111°, 117°, 121°, 124°, 128° and 130°, respectively. Fig. 6(g) displays the quantitative analysis of WCA. The nanocomposite fiber's increased contact angle shows that the hydrophobic nature of the PVDF fiber has been significantly enhanced with the addition

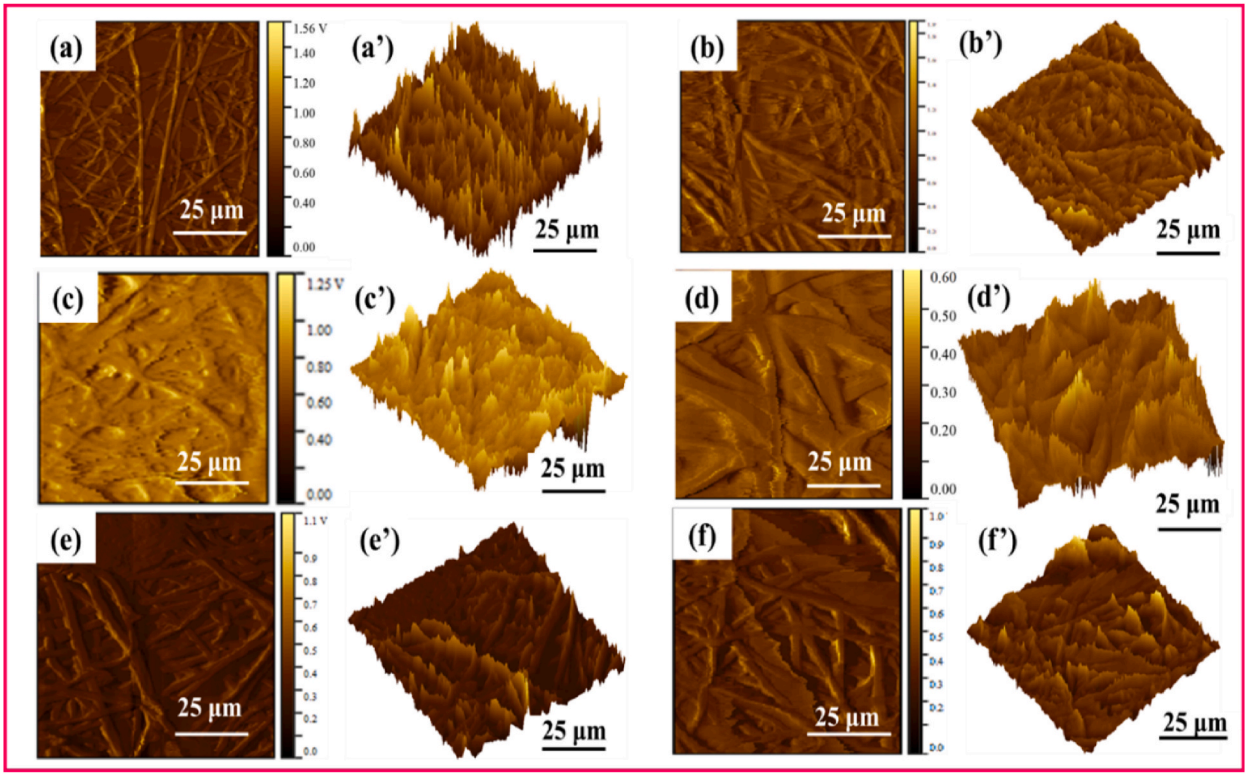

Fig. 5. (a, b, c, d, e and f) High-resolution 2-D AFM images of PN-0, PN-2, PN-4, PN-6, PN-8 and PN-10. (a', b', c', d', e' and f') 3-D AFM images of corresponding fibers.

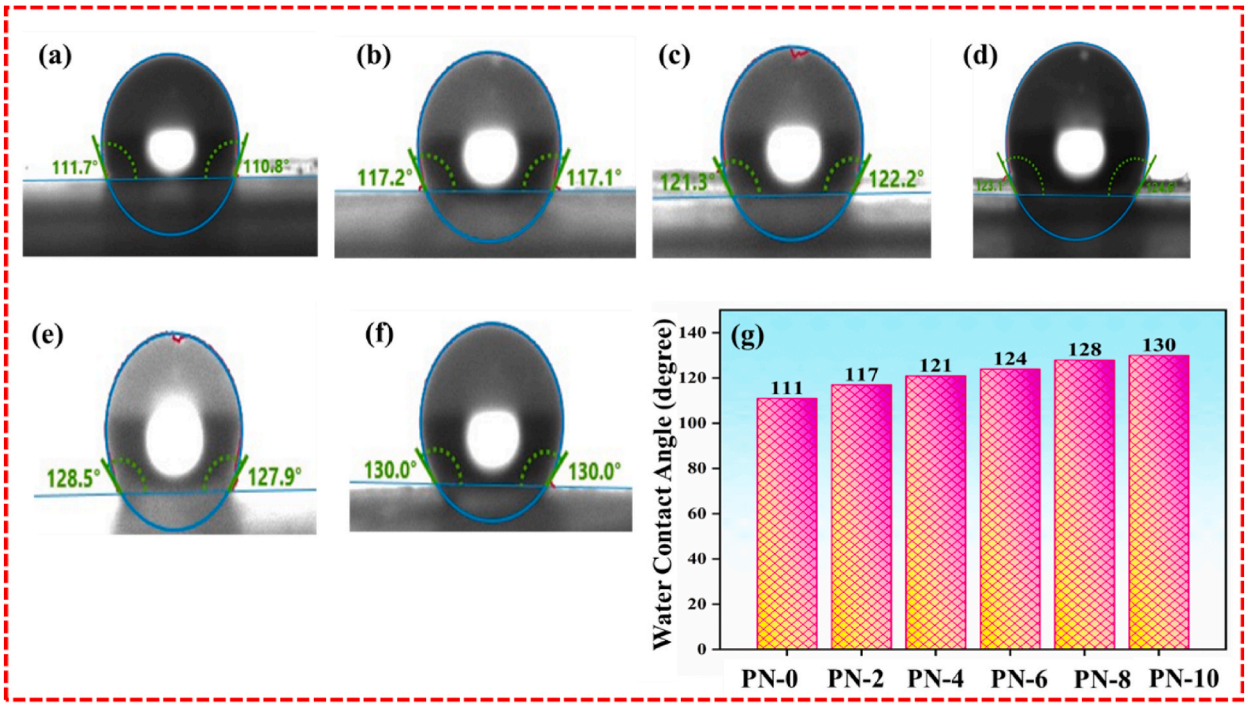

Fig. 6. WCA of (a) PN-0, (b) PN-2, (c) PN-4, (d) PN-6, (e) PN-8 and (f) PN-10 fibers. (g) Quantitative graph of the WCA measurement.

of NiO NP into the PVDF matrix. As a result, the fiber can also be utilized in humid environments. From the Wenzel model, it is concluded that the increased WCA for the PN-6 fiber is due to its high surface roughness, which in turn, increases its hydrophobicity [51,52]. The wettability nature of the fiber is an important factor in day-to-day applications. The hydrophobic nature is the most preferred one, which is confirmed using the WCA study.

3.3. *Mechanism of electroactive β-phase nucleation*

From FTIR and XRD analysis of the composite fibers, doping of NiO NP into the PVDF surface boosts the enhancement of the polar *β*-crystalline phase in PVDF. So, it is important to understand the interaction mechanism of NiO with PVDF matrix. During the NP synthesis step, NaOH was used to maintain the solution pH at 14. According to Xiang et al. [53], the zeta potential value of the NP will vary with the pH of the corresponding precursor solution. The produced NP has a negatively charged surface, which is confirmed by the zeta-potential value at a pH value of 14. The negative-charged NP surface acts as a substrate for the formation of *β*-phase when they are introduced into the PVDF matrix during the solution stage. The negative-charged surface of NP and the partially positively charged $–CH_2$ dipoles have an electrostatic interaction that causes the PVDF chains to align in *all-trans* conformation on the NP surface, leading to the generation of an electroactive *β*-crystalline phase. Thus, the NP's negatively charged surfaces serve as the *β*-phase's nucleation sites. The ion-dipole bonding mechanism between PVDF chains and NiO NP is schematically shown in Fig. 7.

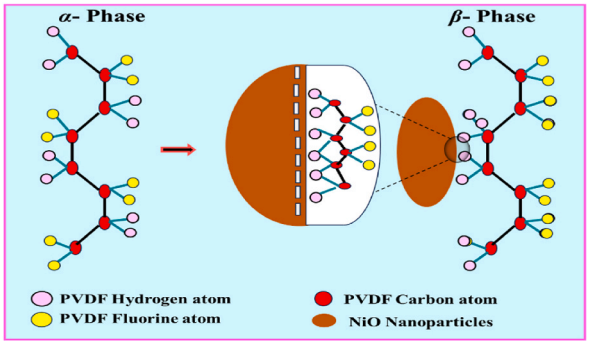

Fig. 7. *β*-phase formation mechanism in NiO-doped PVDF fiber.

3.4. Electrical measurements

The fabricated piezoelectric devices were subjected to an impact under cyclic pressure provided by a customized setup. The produced electrical charge in the conductive Ni/Cu electrodes is collected *via* an additional wire attached to the electrodes. Neat and composite PVDF-based piezoelectric device's $V_{p\text{-}p}$ has been measured under constant force (1.0 kgf) and frequency (1.0 Hz). Since the thickness of prepared fibers significantly affected the output voltage of the sensors, we normalized the $V_{p\text{-}p}$ of the sensors. Neat PVDF based sensor gave an output voltage of 1.0 V, and the composite fiber-based PENG devices gave output voltages (Fig. 8(a–f)) of 2.1 V (PN-2), 2.7 V (PN-4), 3.9 V (PN-6), 2.8 V (PN-8) and 1.6 V (PN-10), and $V_{p\text{-}p}$ of 1.7 V (PN-0), 2.9 V (PN-2), 4.1 V (PN-4), 5.5 V (PN-6), 3.9 V (PN-8) and 2.0 V (PN-10). While doing electrospinning, synchronous poling happened because of the applied high voltage and unidirectional stretching of polymeric chains, which results in an enhanced β-crystalline phase in the fibers. The 6 wt.-% of NiO NP doping into PVDF achieved an 80 % rise in piezoelectric voltage output compared to neat PVDF, which demonstrates that the PN-6 piezoelectric sensor can be effectively used in energy harvesting devices.

Fig. 9(a) shows the quantitative results of the measured voltages. Fig. 9(b–e) shows the additional measurements taken for the optimized device PN-6. Fig. 9(b and c) depicts the fluctuation in the generated voltage by applying a higher force ranging from 2 kgf to 3 kgf at a constant frequency rate of 1.0 Hz. Output voltage generated from increasing the frequency range from 0.1 Hz to 0.5 Hz at a fixed force of 1.0 kgf is depicted in Fig. 9(d and e). The PENG generated 6.5 V and 9.0 V under 2 kgf and 3 kgf, respectively, and with 0.1 Hz and 0.5 Hz frequencies, the PENG generated 3.4 V and 4.4 V, respectively. Fig. 9(f) presents the short circuit current from the different PENG devices. Compared to the PN-0 device (0.7 μA), the composite-based PENG devices showed better output current. PN-2, PN-4, PN-6, PN-8 and PN-10 devices gave a short-circuit current (I_{sc}) of 0.8, 1.07, 1.83, 1.16 and 0.74 μA, respectively.

Additionally, Table 1 presents comparative analyses of our data with PENG sensors designed by other researchers, which indicates better electrical performance of our PN composite PENG. Crystalline nature of the fibers after the electrical measurements is shown in Fig. S1 of SI, which verified that the crystalline characteristics have not changed significantly after applying force. Fig. S2 of SI shows the stability studies of PN-6 based PENG before and after the electrical measurements. The output voltage of PENGs was measured four times continuously with 10-min intervals, and the output response of the PENGs did not show any significant changes, which confirms the stability of the PENG device even after repeated measurements.

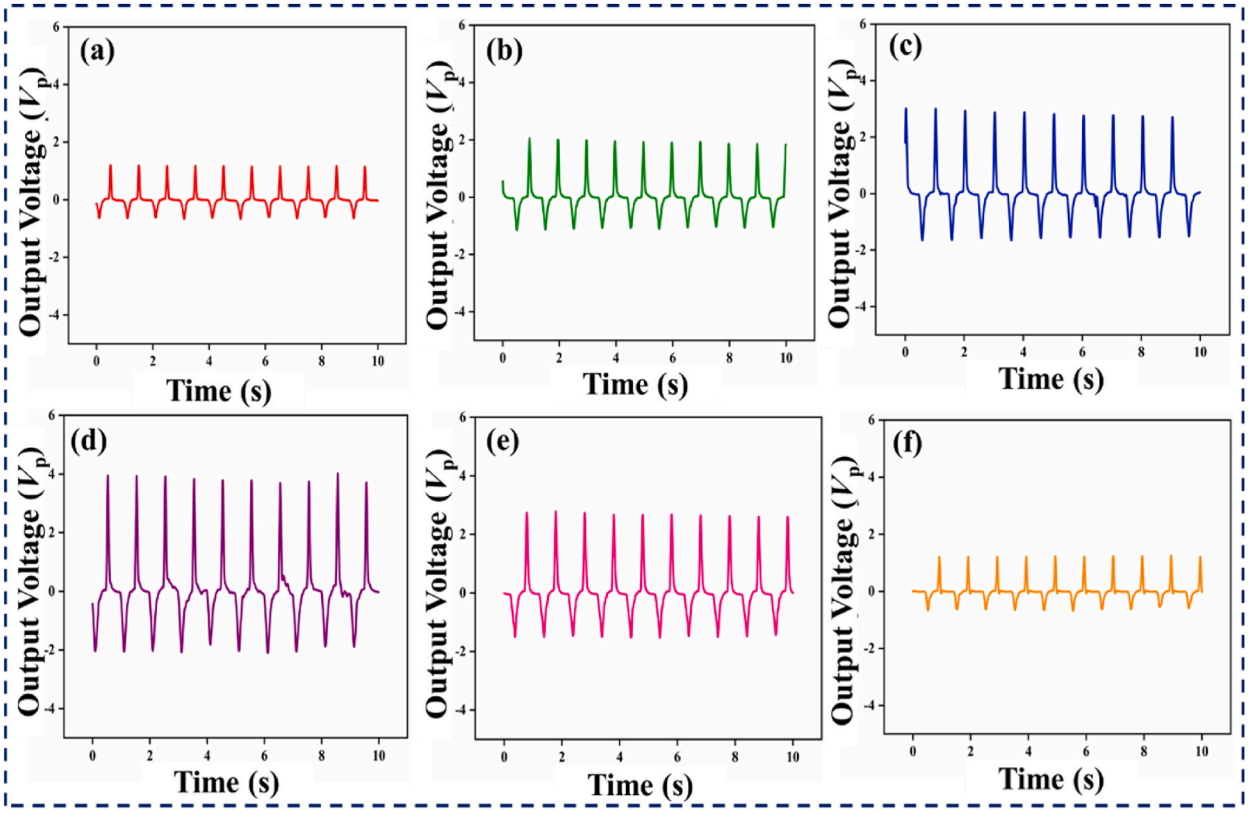

Fig. 8. Piezoelectric output voltage of PENG devices under 1.0 kgf force and 1.0 Hz frequency of (a) PN-0, (b) PN-2, (c) PN-4, (d) PN-6, (e) PN-8 and (f) PN-10.

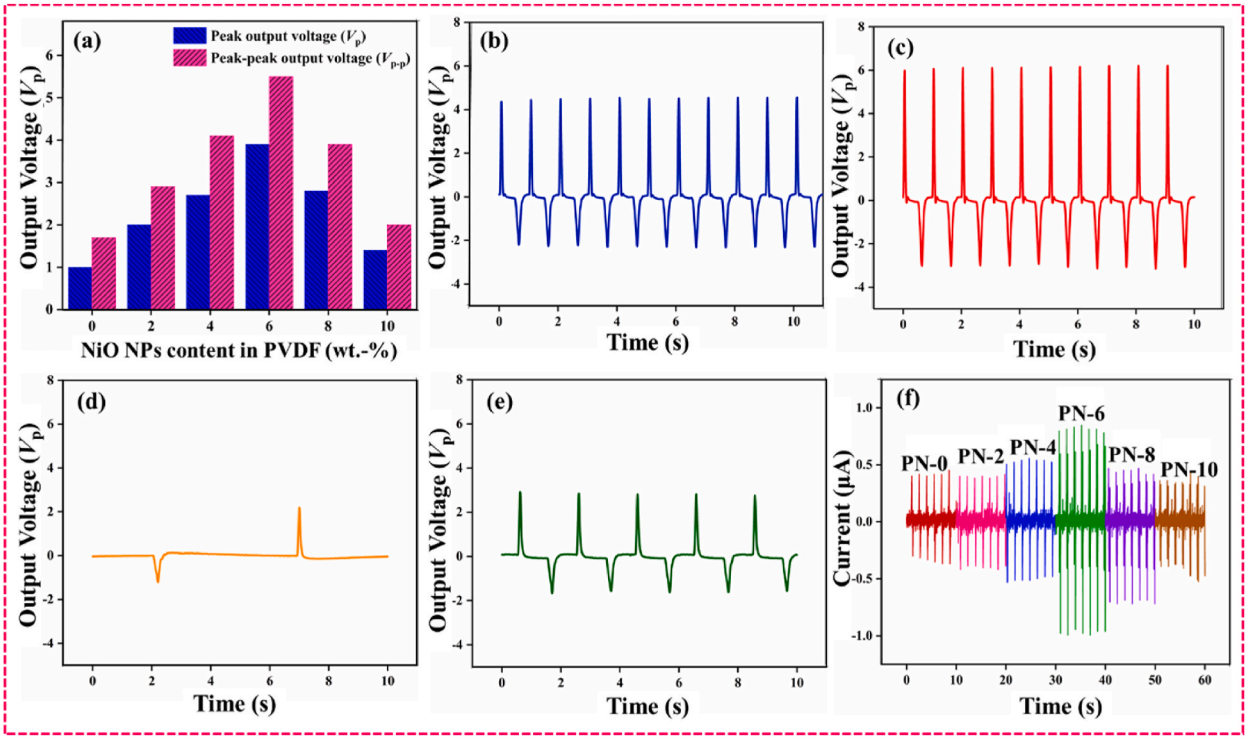

Fig. 9. (a) Quantitative data of output voltage extracted from Fig. 6; V_{p-p} of PN-6 under (b) 2 kgf and 1.0 Hz, (c) 3 kgf and 1.0 Hz, (d) 1 kgf and 0.1 Hz and (e) 1 kgf and 0.5 Hz. (f) Short-circuit current of PN composite based PENG devices.

Table 1
Comparison of previous works of electrospun PVDF-based PENGs.

S. No.	Material	Output Voltage (V)	I_{sc} (μA)	References
1.	PVDF-HFP/HAP	1.1	0.50	[54]
2.	PVDF-ZnO@3-Ag	1.2	–	[55]
3.	PVDF/PET	2.0	0.11	[56]
4.	PVDF/Fe–ZnO	2.4	0.03	[57]
5.	P(VDF-TrFE)/ZnO	2.5	20.8	[58]
6.	PVDF/Cu	2.5	0.37	[6]
7.	PVDF/ZnO	3.0	0.25	[59]
8.	PVDF/PMMA/BT NWs	3.4	0.32	[26]
9.	PVDF/PU	3.8	0.65	[60]
10.	PVDF/TBAHP	4.0	2.04	[61]
11.	PVDF-GO	4.9	0.19	[39]
12.	PVDF-HFP/$NiFe_2O_4$	5.0	–	[54]
13.	PVDF-NiO	5.5	1.83	This work

3.5. Wearable applications

The overall circuit executed for measuring real-time health monitoring and body movements using the Biopac MP 150 instrument is schematically depicted in Fig. 10(a). The optimized flexible PN-6 piezoelectric sensor is placed on a material or in external contact with the human body such as the leg, elbow, fingers, pockets and shoe sole. The performance of piezoelectric sensors is measured at 100 MΩ and an input impedance of 0 Db. As shown in Fig. 10(b), the fabricated sensor produced 8.2 V, 13.1 V, 16.5 V and 10.5 V while tapping, bending, twisting and rolling, respectively (Video S1 in SI). These findings indicate that this piezoelectric sensor reacted more effectively to twisting compared to tapping, bending and rolling. The PENG device is attached to the elbow area for calculating the output voltage produced by the periodic stretching of the arm. Fig. 10(c) depicts the variation in the output voltage during arm movement from 0 to 30° and 0–180°. The output signal of PENG increases dramatically from 12.9 V to 16.4 V when the stretching angle increases from 30° to 180°. Additionally, the device was used as an theft detection sensor as illustrated in Fig. 10(d). Fig. 10(e) shows that an output voltage of 5.6 V measured during walking, and 12.0 V measured during kicking, which is almost two times higher than the voltage measured from walking. Finally, we used the sensor for measuring voltage during walking (12.9 V) and running (15.8 V) by attaching the device to the shoe sole as shown in Fig. 10(f). In contrast to published results, Table 2 indicated that our NiO/PVDF-

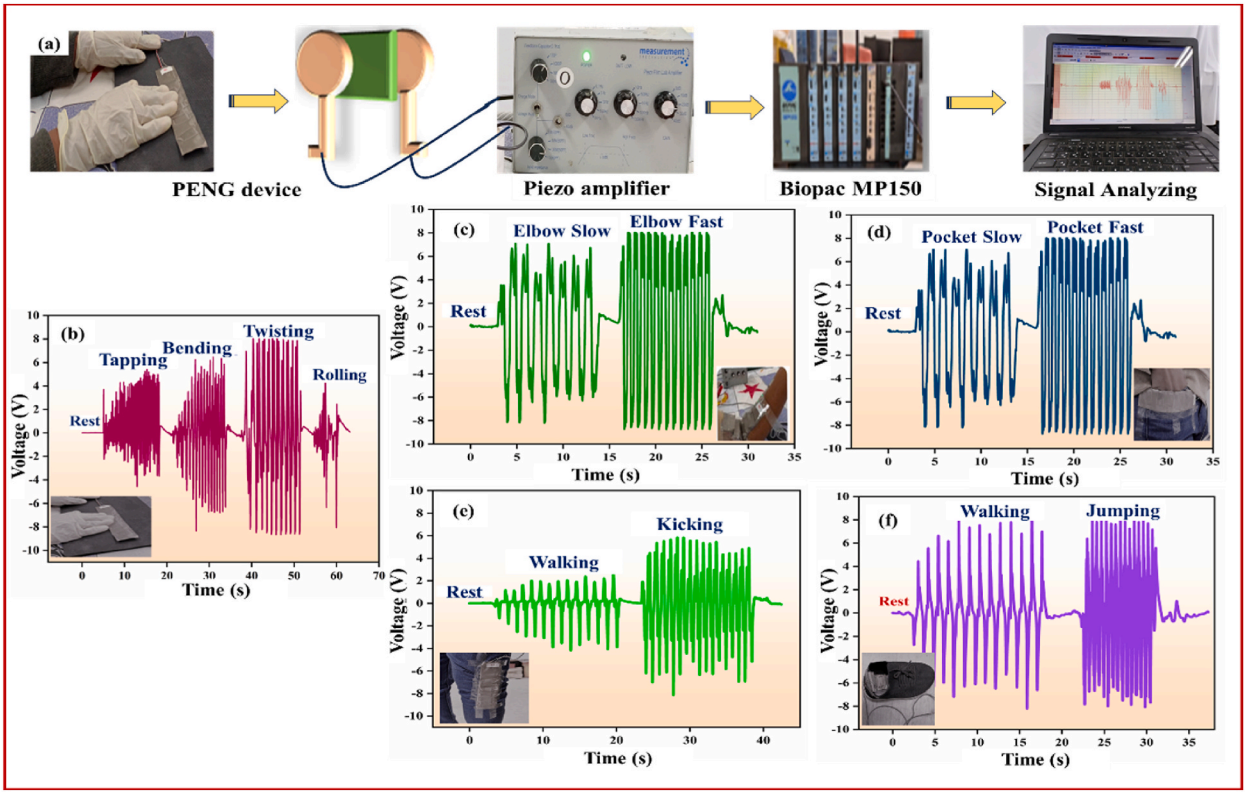

Fig. 10. (a) Graphical illustration of PENG measurement components. Wearable real-time applications of PN-6 PENG under (b) tapping, bending, twisting and rolling, (c) elbow, (d) pocket, (e) leg and (f) shoe sole.

Table 2
Comparative study of the wearable applications of PVDF-based PENG devices.

Material	Wearable application	Output Voltage (V)	Reference
P(VDF-TrFE)/$BaTiO_3$	Walking	6.7	[20]
	Running	7.2	
PVDF/$BaTiO_3$	Palm Tapping	5.2	[17]
	Wrist tapping	2.4	
	Elbow tapping	1.9	
PVDF/Core-shell structured $BaTiO_3$	wrist bending	1.3	[3]
	elbow bending	1.5	
PVDF/ZnO	Shoe sole	3.3	[11]
PVDF/Ce–Fe_2O_3	Wrist movement	0.15	[7]
PVDF/$BiCl_3$/ZnO	Elbow bending	3.0	[33]
	Knee bending	0.6	
PVDF/NiO	Tapping	8.2	This work
	Bending	13.1	
	Twisting	16.5	
	Rolling	10.5	
	Elbow bending	12.9	
	Walking	5.6	
	Running	15.8	

based PENG devices provided superior output performance in wearable applications. From these findings, the proposed PENG device is demonstrated to have wider applications in the area of neurological treatment, especially for facilitating hand recovery and training for walking after stroke or any severe brain damage.

4. Conclusions

This paper discusses the synthesis of NiO NPs, electrospinning of NiO doped PVDF (PN-0 to 10), PENG device fabrication based on the electrospun nanofiber and their wearable application studies. SEM analysis confirmed the uniform dispersion of NP in the PVDF

matrix and the even structure of NFs. Studies from XRD and FTIR analysis established the influence of NiO NP towards enhancing the β-phase in PVDF. Compared to neat PVDF fiber (58 %), doping of 6 wt.-% NiO NP in PVDF (PN-6) resulted in an enhanced polar phase (70 %), and the percentage of polar β-phase starts to decrease for higher NiO content (PN-8 and PN-10). The role of NiO NP in enhancing the PENG's piezoelectric efficiency is demonstrated for real-time uses. $V_{p\text{-}p}$ of 5.5 V was obtained for PN-6, which is 3.5 times greater than the voltage generated from the PN-0 device (1.7 V) under a 1.0 kgf force and 1.0 Hz frequency. Also, the short-circuit current of the PN-6 device (1.83 μA) is 2.5 times greater than that of the PN-0 device (0.7 μA). Up to now, PENG devices' primary drawback has been their low output performance. Lastly, the developed PENG devices were used to identify gestures like walking, running, kicking, tapping and elbow movements. After comparing our sensor's wearable performance with previously reported data, it was determined that the PVDF/NiO PENG device displayed higher voltages. The developed PENG device can be used in the area of neurological treatment, especially for facilitating hand recovery and training for walking after a stroke or any severe brain damage. On that account, this device has versatile applications in the medical field.

Informed consent statement

Patient consent was waived as all the measurements reported in this work is only applicable for external use in the human body and not internally. The sensor is placed externally to the subject (B.A.) and integrated into clothes and accessories. This study is not harmful to the human body.

Data availability statement

Has data associated with your study been deposited into a publicly available repository? NO Data will be made available on request.

CRediT authorship contribution statement

Bindhu Amrutha: Writing – original draft, Methodology. **Arun Anand Prabu:** Writing – review & editing, Supervision. **Madhvesh Pathak:** Validation, Supervision.

Declaration of competing interest

The authors declare the following financial interests/personal relationships which may be considered as potential competing interests: Arun Anand Prabu has patent pending to IQAC VIT. If there are other authors, they declare that they have no known competing financial interests or personal relationships that could have appeared to influence the work reported in this paper.

Acknowledgments

This publication was made possible by 'MHRD-SPARC, India (No. 2018–2019/P399)'. The authors also thank VIT for providing a 'VIT SEED GRANT (SG20230088 dt. June 23, 2023)' for carrying out this research work. The authors are grateful to Prof. Hongdoo Kim and Prof. Kap Jin Kim, Kyung Hee University, Republic of Korea for providing the piezoelectric measurement facility and to Dr. Mohammad Shamim Reza for assisting the piezoelectric measurements in their facility.

Appendix A. Supplementary data

Supplementary data to this article can be found online at https://doi.org/10.1016/j.heliyon.2024.e29192.

References

[1] D. Masekela, N.C. Hintsho-Mbita, S. Sam, T.L. Yusuf, N. Mabuba, Application of $BaTiO_3$-based catalysts for piezocatalytic, photocatalytic and piezo-photocatalytic degradation of organic pollutants and bacterial disinfection in wastewater: a comprehensive review, Arab. J. Chem. 16 (2023) 104473, https://doi.org/10.1016/j.arabjc.2022.104473.

[2] M. Zahid, H.A. Rathore, H. Tayyab, Z.A. Rehan, I.A. Rashid, M. Lodhi, U. Zubair, I. Shahid, Recent developments in textile-based based polymeric smart sensor for human health monitoring: a review, Arab. J. Chem. 15 (2022) 103480, https://doi.org/10.1016/j.arabjc.2021.103480.

[3] S. Wang, Z. Yu, L. Wang, Y. Wang, D. Yu, M. Wu, A core-shell structured barium titanate nanoparticles for the enhanced piezoelectric performance of wearable nanogenerator, Appl. Energy 351 (2023) 121835, https://doi.org/10.1016/j.apenergy.2023.121835.

[4] S. Yempally, P. Magadia, D. Ponnamma, Effect of Zn-Fe_2O_3 nanomaterials on the phase-separated morphologies of polyvinylidene fluoride piezoelectric nanogenerators, RSC Adv. 13 (2023) 33863, https://doi.org/10.1039/d3ra03745b.

[5] N.H. Kamsani, M.S. Haris, M. Pandey, M. Taher, K. Rullah, Biomedical application of responsive 'smart' electrospun nanofibers in drug delivery system: a minireview, Arab. J. Chem. 14 (2021) 103199, https://doi.org/10.1016/j.arabjc.2021.103199.

[6] S. Wang, Z. Yu, Y. He, C. Li, L. Wang, M. Wu, A fabric-based electrode for wearable piezoelectric nanogenerators to distinguish sense human motions, Appl. Surf. Sci. 610 (2023) 11, https://doi.org/10.1016/j.apsusc.2022.155451.

[7] H. Parangusan, D. Ponnamma, M.A.A. AlMaadeed, Toward high power generating piezoelectric nanofibers: influence of particle size and surface electrostatic interaction of Ce-Fe_2O_3 and Ce-Co_3O_4 on PVDF, ACS Omega 4 (4) (2019) 6312–6323, https://doi.org/10.1021/acsomega.9b00243.

[8] J. Kharade, H. Vasquez, K. Lozano, Enhanced piezoelectric performance of aligned PVDF electrospun fiber mats, Emergent Mater 5 (1) (2022) 187–193, https://doi.org/10.1007/s42247-021-00332-0.

[9] S.S. Shah, M.A. Aziz, A.R. Al-Betar, W. Mahfoz, Electrodeposition of polyaniline on high electroactive indium tin oxide nanoparticles-modified fluorine-doped tin oxide electrode for fabrication of high-performance hybrid supercapacitor, Arab. J. Chem. 15 (2022) 104058, https://doi.org/10.1016/j.arabjc.2022.104058.

[10] A. Pal, A. Sasmal, B. Manoj, D.S.D.P. Rao, A.K. Haldar, S. Sen, Enhancement in energy storage and piezoelectric performance of three-phase (PZT/MWCNT/PVDF) composite, Mater. Chem. Phys. 244 (2020) 122639, https://doi.org/10.1016/j.matchemphys.2020.122639.

[11] A. Mahapatra, R.S. Ajimsha, M.O. Ittoop, A. Sharma, S. Karmakar, A. Shaikh, P.R. Sankar, P. Misra, Flexible ZnO: PVDF-based free-standing piezoelectric nanogenerator for vibrational energy harvesting and wearable shoe insole pedometer sensor, J. Alloys Compd. 960 (2023) 170898, https://doi.org/10.1016/j.jallcom.2023.170898.

[12] C. Yu, J. Xu, L. Yang, H. Wang, T. Li, Y. Ye, G. Rao, Paper-based piezoelectric sensors with an irregular porous structure constructed by scraping of 3D $BaTiO_3$ particles/Poly(vinylidene fluoride) for micro pressure and human motion sensing, Sens. Actuator A Phys. 357 (2023) 114395, https://doi.org/10.1016/j.sna.2023.114395.

[13] H.B. Kang, J. Chang, K. Koh, L. Lin, Y.S. Cho, High-quality Mn-doped $(Na,K)NbO_3$ nanofibers for flexible piezoelectric nanogenerators, ACS Appl. Mater. Interfaces 13 (2014) 10576–10582, https://doi.org/10.1021/am502234q.

[14] T. Wu, Y. Song, Z. Shi, D. Liu, S. Chen, C. Xiong, Q. Yang, High-performance nanogenerators based on flexible cellulose nanofibril/MoS_2 nanosheet composite piezoelectric films for energy harvesting, Nano Energy 80 (2021) 105541, https://doi.org/10.1016/j.nanoen.2020.105541.

[15] Y. Guan, M. Bai, Q. Wang, L. Liu, S. Yu, B. Kong, F. Lv, M. Guo, G. Liu, L. Li, L. Zhang, Y. Lin, W. Li, A self-powered wearable piezoelectric nanogenerator for physiological monitoring based on lead zirconate titanate/microfibrillated cellulose@polyvinyl alcohol (PZT/MFC@PVA) composition, Chem. Eng. J. 460 (2023) 141598, https://doi.org/10.1016/j.cej.2023.141598.

[16] Y. Zheng, W. Wang, J. Niu, X. Jin, Y. Sun, L. Peng, W. Li, H. Wang, T. Lin, Thermoacoustic energy harvesting using thermally-stabilized polyacrylonitrile nanofibers, Nano Energy 95 (2022) 106995, https://doi.org/10.1016/j.nanoen.2022.106995.

[17] M. Kumar, N.D. Kulkarni, P. Kumari, Piezoelectric performance enhancement of electrospun functionally graded PVDF/$BaTiO_3$ based flexible nanogenerators, Mater. Res. Bull. 174 (2024) 112739, https://doi.org/10.1016/j.materresbull.2024.112739.

[18] R. Mitra, B.S. Priyadarshini, A. Ramadoss, U. Manju, Stretchable polymer-modulated PVDF-HFP/TiO_2 nanoparticles-based piezoelectric nanogenerators for energy harvesting and sensing applications, Mater. Sci. Eng. B 286 (2022) 116029, https://doi.org/10.1016/j.mseb.2022.116029.

[19] D. Mandal, K. Henkel, D. Schmeiber, Improved performance of a polymer nanogenerator based on silver nanoparticles doped electrospun P(VDF-HFP) nanofibers, Phys. Chem. Chem. Phys. 16 (2014) 10403–10407, https://doi.org/10.1039/C3CP55238A.

[20] X. Guan, B. Xu, J. Gong, Hierarchically architected polydopamine-modified $BaTiO_3$@P(VDF-TrFE) nanocomposite fiber mats for flexible piezoelectric nanogenerators and self-powered sensors, Nano Energy 70 (2020) 104516, https://doi.org/10.1016/j.nanoen.2020.104516.

[21] W.H. Han, M.Q. Wang, J.X. Yuan, C.C. Hao, C.J. Li, Y.Z. Long, S. Ramakrishna, Electrospun aligned nanofibers: a review, Arab. J. Chem. 15 (2022) 104193, https://doi.org/10.1016/j.arabjc.2022.104193.

[22] Y. Zhai, J. Yang, Fabrication and modification of PVDF membrane by PDA@ZnO for enhancing hydrophilic and antifouling property, Arab. J. Chem. 16 (2023) 105206, https://doi.org/10.1016/j.arabjc.2023.105206.

[23] X. Zheng, L. He, G. Yu, H. Wang, H. Fu, H. Huang, Sequentially-excited multi-oscillator piezoelectric rotary energy harvester for charging capacity enhancement, Sustain. Energy Technol. Assess. 60 (2023) 103487, https://doi.org/10.1016/j.seta.2023.103487.

[24] D.M. Dhevi, A.A. Prabu, M. Pathak, Miscibility, crystallization and annealing studies of poly (vinylidene fluoride)/hyperbranched polyester blends, Polymer 55 (2014) 886–895, https://doi.org/10.1016/j.polymer.2013.12.048.

[25] D.M. Dhevi, A.A. Prabu, K.J. Kim, Infrared spectroscopic studies on crystalline phase transition of PVDF and PVDF/hyperbranched polyester blend ultrathin films, Vib. Spectrosc. 94 (2017) 74–82, https://doi.org/10.1016/j.vibspec.2017.12.003.

[26] B. Zhao, Z. Chen, Z. Cheng, S. Wang, T. Yu, W. Yang, Y. Li, Piezoelectric nanogenerators based on electrospun PVDF-coated mats composed of multilayer polymer-coated $BaTiO_3$ nanowires, ACS Appl. Nano Mater. 5 (2022) 8417–8428, https://doi.org/10.1021/acsanm.2c01538.

[27] B. Amrutha, G. Prasad, P. Sathiyanathan, M.S. Reza, H. Kim, M. Pathak, A.A. Prabu, Fabrication of CuO-NP-doped PVDF composites based electrospun triboelectric nanogenerators for wearable and biomedical applications, Polymers 11 (2023) 1–15, https://doi.org/10.3390/polym15112442.

[28] Y. Qiu, S. Sun, X. Wang, K. Shi, Z. Wang, X. Ma, W. Zhang, G. Bao, Y. Tian, Z. Zhang, H. Ding, H. Chai, A. Liu, H. Wu, Nondestructive identification of softness *via* bioinspired multisensory electronic skins integrated on a robotic hand, NPJ Flex. Electro. 45 (2022) 3556, https://doi.org/10.1038/s41528-022-00181-9.

[29] C. Ribeiro, C.M. Costa, D.M. Correia, J.N. Pereira, J. Oliveira, P. Martins, R. Goncalves, V.F. Cardoso, S.L. Mendez, Electroactive poly(vinylidene fluoride)-based structures for advanced applications, Nat. Protoc. 13 (2018) 681–704, https://doi.org/10.1038/nprot.2017.157.

[30] I.S. Goncalves, J.A.V. Costa, M.G. Morais-de, Microfiltration membranes developed from nanofibers *via* an electrospinning process, Mater. Chem. Phys. 277 (2022) 125509, https://doi.org/10.1016/j.matchemphys.2021.125509.

[31] M. Sharma, G. Madras, S. Bose, Process induced electroactive β-polymorph in PVDF: effect on dielectric and ferroelectric properties, Phys. Chem. Chem. Phys. 16 (2014) 14792–14799, https://doi.org/10.1039/C4CP01004C.

[32] A. Gebrekrstos, M. Sharma, G. Madras, S. Bose, New physical insights into shear history dependent polymorphism in PVDF, Cryst. Growth Des. 16 (2016) 2937–2944, https://doi.org/10.1021/acs.cgd.6b00282.

[33] D. Zhang, X. Zhang, X. Li, H. Wang, X. Sang, G. Zhu, Y. Yeung, Enhanced piezoelectric performance of PVDF/$BiCl_3$/ZnO nanofiber-based piezoelectric nanogenerator, Eur. Polym. J. 166 (2022) 110956, https://doi.org/10.1016/j.eurpolymj.2021.110956.

[34] D.R. Lei, N. Hu, L. Wu, H. Ning, Y. Wang, Z. Jin, Improvement of the piezoelectricity of PVDF-HFP by $CoFe_2O_4$ nanoparticles, Nano Mater. Sci. (2023) 2589–9651, https://doi.org/10.1016/j.nanoms.2023.03.002.

[35] N.D. Kulkarni, P. Kumari, Development of highly flexible PVDF-TiO_2 nanocomposites for piezoelectric nanogenerator applications, Mater. Res. Bull. 157 (2023) 112039, https://doi.org/10.1016/j.materresbull.2022.112039.

[36] A.M. Al-Enizi, M.M. El-Halwany, S.F. Shaikh, B. Pandit, A. Yousel, Electrospun nickel nanoparticles@poly(vinylidene fluoride-hexafluoropropylene) nanofibers as effective and reusable catalyst for H_2 generation from sodium borohydride, Arab. J. Chem. 15 (2022) 104207, https://doi.org/10.1016/j.arabjc.2022.104207.

[37] F. Yalcinkaya, Preparation of various nanofiber layers using wire electrospinning system, Arab. J. Chem. 12 (2019) 5162–5172, https://doi.org/10.1016/j.arabjc.2016.12.012.

[38] D. Dhakras, V. Borkar, S. Ogale, J. Jog, Enhanced piezoresponse of electrospun PVDF mats with a touch of nickel chloride hexahydrate salt, Nanoscale 4 (2012) 752–756, https://doi.org/10.1039/C2NR11841F.

[39] G. Chen, L. Pan, D. Chen, Electrospun flexible PVDF/GO piezoelectric pressure sensor for human joint monitoring, Diam. Relat. Mater. 129 (2022) 109358, https://doi.org/10.1016/j.diamond.2022.109358.

[40] S. Bairagi, S.W. Ali, A hybrid piezoelectric nanogenerator comprising of KNN/ZnO nanorods incorporated PVDF electrospun nanocomposite webs, Int. J. Energy Res. 44 (2020) 1–19, https://doi.org/10.1002/er.5306.

[41] B. Dutta, N. Bose, E. Kar, S. Das, S. Mukherjee, Smart, lightweight, flexible NiO/poly(vinylidene fluoride) nanocomposites film with significantly enhanced dielectric, piezoelectric and EMI shielding properties, J. Polym. Res. 24 (2018) 220, https://doi.org/10.1007/s10965-017-1396-z.

[42] B. Dutta, E. Kar, G. Sen, N. Bose, S. Mukherjee, Lightweight, flexible NiO@SiO_2/PVDF nanocomposite film for UV protection and EMI shielding application, Mater. Res. Bull. 124 (2020) 110746, https://doi.org/10.1016/j.materresbull.2019.110746.

[43] H.M. Venkatesan, A.P. Arun, Nickel-oxide-doped polyvinylidene fluoride nanofiber-based flexible triboelectric nanogenerator for energy harvesting and healthcare monitoring applications,. ACS Appl. Electron. Mater. https://doi.org/10.1021/acsaelm.3c01551.

[44] A. Rahdar, M. Aliahmad, Y. Azizi, NiO nanoparticles: synthesis and characterization, J. Nanostruct. 5 (2015) 145–151, https://doi.org/10.7508/jns.2015.02.009.

[45] M.I. Rahmah, E.T. Garallah, Preparation of copper oxides/polyvinyl alcohol nanocoatings with antibacterial activity, Chem. Data Collect. 39 (2022) 100869, https://doi.org/10.1016/j.cdc.2022.100869.
[46] R. Gunasekhar, A.A. Prabu, Fabrication of 1st generation aromatic hyperbranched polyester/polyvinylidene fluoride blended electrospun composites to enrich the piezoelectric performance, J. Polym. Res. 287 (2023) 1–10, https://doi.org/10.1007/s10965-023-03675-w.
[47] G. Prasad, X. Lin, J. Liang, Y. Yao, T. Tao, B. Liang, S.G. Lu, Fabrication of intra-porous PVDF fibers and their applications for heavy metal removal, oil absorption, and piezoelectric sensors, J. Materiomics. 9 (2023) 174–182, https://doi.org/10.1016/j.jmat.2022.08.003.
[48] P. Thakur, A. Kool, N.A. Hoque, B. Bagchi, F. Khatun, P. Biswas, D. Brahma, S. Roy, S. Banerjee, S. Das, Superior performances of in situ synthesized ZnO/PVDF thin film based self-poled piezoelectric nanogenerator and self-charged photo-power bank with high durability, Nano Energy 44 (2018) 456–467, https://doi.org/10.1016/j.nanoen.2017.11.065.
[49] P. Martins, A.C. Lopes, S.L. Mendez, Electroactive phases of poly(vinylidene fluoride): determination, processing, and applications, Prog. Polym. Sci. 39 (2014) 683–706, https://doi.org/10.1016/j.progpolymsci.2013.07.006.
[50] G. Prasad, J.U. Yoon, I. Woo, J.W. Bae, Fabrication of amino and fluorine functionalized graphene-based polymer composites to enhance the electrochemical conversion efficiency of TENGs for energy-harvesting applications, Chem. Eng. J. 470 (2023) 144280, https://doi.org/10.1016/j.cej.2023.144280.
[51] R.N. Wenzel, Resistance of solid surfaces to wetting by water, Ind. Eng. Chem. 28 (1936) 988–994, https://doi.org/10.1021/ie50320a024.
[52] M.I. Rahmah, R.S. Sabry, W.J. Aziz, Preparation and antibacterial activity of superhydrophobic modified ZnO/PVC nanocomposite, J. Bionic Eng. 19 (2022) 139–154, https://doi.org/10.1007/s42235-021-00106-8.
[53] L. Xiang, X.Y. Deng, Y. Jin, Experimental study on the synthesis of NiO nanoparticles, Scr. Mater. 47 (2002) 219–224, https://doi.org/10.1016/S1359-6462(02)00108-2.
[54] S. Wang, W. Tong, Y. Li, P. Zhang, Y. Liu, Y. Chen, Y. Zhang, Contributions of piezoelectricity and triboelectricity to a hydroxyapatite/PVDF-HFP fiber-film nanogenerator, Nano Energy 105 (2023) 108026, https://doi.org/10.1016/j.nanoen.2022.108026.
[55] O.M. Zeyrek, S. Oguzlar, U. Kartal, M. Yurddaskal, O. Cihanbegendi, Energy harvesting nanogenerators: electrospun β-PVDF nanofibers accompanying ZnO NPs and ZnO@Ag NPs, Solid State Sci. 122 (2021) 106772, https://doi.org/10.1016/j.solidstatesciences.2021.106772.
[56] D.B. Kim, J. Han, S.M. Sung, M.S. Kim, B.K. Choi, S.J. Park, H.R. Hong, H.J. Choi, B.K. Kim, C.H. Park, J.H. Paik, J.S. Lee, Y.S. Cho, Weave-pattern-dependent fabric piezoelectric pressure sensors based on polyvinylidene fluoride nanofibers electrospun with 50 nozzles, NPJ Flexible Electronics 6 (2022) 69, https://doi.org/10.1038/s41528-022-00203-6.
[57] H. Parangusan, D. Ponnamma, M.A.A. AlMaadeed, Investigation on the effect of γ-irradiation on the dielectric and piezoelectric properties of stretchable PVDF/Fe-ZnO nanocomposites for self-powering devices, Soft Matter 14 (2018) 8803–8813, https://doi.org/10.1039/C8SM01655K.
[58] M. Kumar, P. Kumari, P. Sahatiya, P(VDF-TrFE)/ZnO nanofiber composite based piezoelectric nanogenerator as self-powered sensor: fabrication and characterization, J. Polym. Res. 29 (2022) 44, https://doi.org/10.1007/s10965-022-02890-1.
[59] S. Mirjalali, R. Bagherzadeh, S. Abrishami, M. Asadnia, S. Huang, A. Michael, S. Peng, C.H. Wang, S. Wu, Multilayered electrospun/electrosprayed polyvinylidene fluoride plus zinc oxide nanofiber mats with enhanced piezoelectricity, Macromol. Mater. Eng. 308 (2023) 2300009, https://doi.org/10.1002/mame.202300009.
[60] D. Ponnamma, O. Aljarod, H. Parangusan, M.A.A. Al-Maadeed, Electrospun nanofibers of PVDF-HFP composites containing magnetic nickel ferrite for energy harvesting application, Mater. Chem. Phys. 239 (2020) 122257, https://doi.org/10.1016/j.matchemphys.2019.122257.
[61] Y. Zhao, M. Jia, X. Wang, X. Sun, Z. Li, Enhanced output performance piezoelectric nanogenerators based on highly polarized PVDF/TBAHP tree-like nanofiber membranes for energy harvesting, Polymer 293 (2024) 126681, https://doi.org/10.1016/j.polymer.2024.126681.